Phases and collective modes of Rydberg atoms in an optical lattice

K. Saha,[1] S. Sinha,[2] and K. Sengupta[1]
[1]*Theoretical Physics Department, Indian Association for the Cultivation of Science, Jadavpur, Kolkata 700032, India*
[2]*Indian Institute of Science Education and Research, Kolkata, Mohanpur, Nadia 741252, India*
(Received 14 August 2013; published 14 February 2014)

We chart out the possible phases of laser-driven Rydberg atoms in the presence of a hypercubic optical lattice. We define a pseudospin degree of freedom whose up (down) components correspond to the excited (ground) states of the Rydberg atoms and use them to demonstrate the realization of a canted Ising antiferromagnetic (CIAF) Mott phase of the atoms in these systems. We also show that, on lowering the lattice depth, the quantum melting of the CIAF and density-wave Mott states (which are also realized in these systems) leads to supersolid phases of the atoms. We provide analytical expressions for the phase boundaries and collective excitations of these phases in the hard-core limit within mean-field theory and discuss possible experiments to test our theory.

DOI: 10.1103/PhysRevA.89.023618 PACS number(s): 67.85.−d, 03.75.Lm, 05.30.Jp, 05.30.Rt

I. INTRODUCTION

The study of ultracold atoms which can be excited to Rydberg states by suitable laser driving has generated both experimental and theoretical interest in recent years [1–12]. Such excited states are known to have large polarizability, which leads to strong van der Waals force between them. This leads to suppression of additional Rydberg excitations within a fixed radius of an already excited atom; such a phenomenon, known as a dipole blockade, has been theoretically proposed [1] and experimentally verified [2]. Furthermore, such systems have also been widely studied due to their potential for generating exotic many-body ground states. The presence of van der Waals interaction between the excited atoms in these systems has been recognized as an additional source of long-range interaction ($\sim 1/r^6$) between the excited atoms. It was shown that such an interaction may lead to supersolid (SS) droplets within a superfluid (SF) phase of these atoms [3] and may drive a second-order phase transition between their uniform SF and crystalline SS phases [4]. The coherent collective excitation of a SF phase in the presence of such Rydberg excitations has also been studied [5]. Furthermore, it has been theoretically conjectured that such systems may act as quantum simulators and can thus be used to realize qubits [6]. More recently, the physics of these atoms in low-dimensional optical lattices was studied; it was shown that the presence of such a lattice leads to several interesting effects such as a staircase structure in the number of excited atoms [7], one-dimensional (1D) ground states which host non-Abelian excitations such as Fibonacci anyons [8], the realization of exotic spin models with collective fermionic excitations [9], the dynamic creation of molecular states of such atoms [10], and the realization of the hard-square model in the Mott-insulating (MI) state of two-dimensional lattices [11]. The superfluidity of Rydberg atoms in a 1D optical lattice was also experimentally studied [12]; it was shown that a SF phase of such a system in the presence of a lattice can exist in spite of the presence of the van der Waals interaction. However, a system of such Rydberg atoms in higher-dimensional optical lattices has not been studied theoretically so far.

In this work, we study a system of such Rydberg atoms characterized by a laser drive frequency Ω, a detuning parameter Δ, and a van der Waals interaction strength $V_{\rm di}$ in the presence of a hypercubic optical lattice. We present a phase diagram of such a system and demonstrate the presence of a translational-symmetry broken density wave (DW) and a canted Ising antiferromagnetic (CIAF) [where the pseudospin up (down) states correspond to the excited (ground) states of the Rydberg atoms] Mott phases. We note that such a CIAF phase amounts to realization of a higher-dimensional translational-symmetry broken spin-ordered ground state using ultracold atoms [13]. On lowering the lattice depth starting from these DW or CIAF Mott phases, the atoms undergo successive quantum phase transitions to SS and SF phases. We provide analytic expressions for the above-mentioned phase boundaries in the hard-core limit within a mean-field theory and compute their collective excitations. We point out that these collective excitations in the SS phase, reached by increasing hopping strength of the atoms from the CIAF, constitute a mixing of the holelike excitations with the pseudospin collective modes. This is in contrast to the SS phase obtained analogously from the DW Mott state, where these modes do not hybridize and thus these excitations provide a way to distinguish between these two SS phases. We discuss possible experiments to test our theory. We note that the properties of ultracold atoms with Rydberg excitations in a higher-dimensional optical lattice has not been studied so far; our results, particularly the existence of DW, CIAF, and SS phases, are therefore expected to be of interest to both experimentalists and theorists working in these fields.

The paper is organized as follows. In Sec. II, we study the model Hamiltonian describing the system of Rydberg atoms and present a phase diagram of such a system. This is followed by a detailed study of various phases and collective excitations of Rydberg atoms in the hard-core limit presented in Sec. III. Finally, we discuss experiments which can test our theory and conclude in Sec. IV and present details of our calculation in the Appendix.

II. THE MODEL AND PHASE DIAGRAM

We begin with an effective Hamiltonian of the system of ultracold bosonic atoms in an optical lattice, coupled to a highly excited Rydberg state, given

by $H = H_0 + H_1 + H_2$ [7], where

$$H_0 = \Omega \sum_i (a_i^\dagger b_i + \text{H.c.}) - \mu \sum_i \hat{n}_i + \Delta \sum_i \hat{n}_i^b + U \sum_i \hat{n}_i^a (\hat{n}_i^a - 1) + \lambda U \sum_i \hat{n}_i^a \hat{n}_i^b,$$

$$H_1 = -J/2 \sum_{\langle ij \rangle} (a_i^\dagger a_j + \eta b_i^\dagger b_j + \text{H.c.})$$

$$H_2 = V_{\text{di}}/2 \sum_{ij} (\hat{n}_i^b \hat{n}_j^b)/|i-j|^6. \quad (1)$$

Here a_i (b_i) denotes creation operators for the bosons in the ground (excited) state at the lattice site i, $\hat{n}_i^{a(b)} = a_i^\dagger a_i$ ($b_i^\dagger b_i$) are the corresponding number operators, and μ is the chemical potential. The on-site part of the Hamiltonian is described by H_0, where U (λU) is the on-site interaction strength between two bosons in ground (different) states. In a typical experiment the atoms are excited to Rydberg states of very large quantum numbers by two photon excitations. The first part of H_0 describes the coupling between the ground and Rydberg excited states with an effective Rabi frequency Ω [14]. The center-of-mass motion of the atoms is described by H_1, where $\langle ij \rangle$ indicates that j is one of the nearest-neighbor sites of i, J (ηJ) is the nearest-neighbor hopping amplitude of the bosons in the ground (excited) states which can be tuned by tuning the optical lattice depth, and we have set the lattice spacing to unity. The last part of the Hamiltonian H_3 describes van der Waals repulsion between the Rydberg excited states. We assume that the van der Waals interaction between the Rydberg atoms is strong enough to allow $n_i^b \leqslant 1$ at each site, but it can be neglected for $|i-j| \geqslant 2$: $z(z-1)V_{\text{di}}/32 \leqslant \Omega, \Delta, U$, where $z = 2d$ denotes the coordination number of the lattice. In this regime, it is possible to approximate the long-range interaction term by $H_2 \simeq V_{\text{di}}/2 \sum_{\langle ij \rangle} \hat{n}_i^b \hat{n}_j^b$ [15].

We begin our analysis within a mean-field (MF) analysis of the Hamiltonian [Eq. (1)], which turns out to be a reasonable method to describe the MI-SF transition for ultracold bosons. The prediction of the mean-field theory is well known to qualitatively agree with both experimental results and quantum Monte Carlo data for $d \geqslant 2$. However, MF approximation breaks down for $d < 2$ due to strong quantum fluctuations and we do not expect our analysis to hold for $d = 1$. The simplest variational Gutzwiller wave function which can describe the phases of such a system is given by $|\psi\rangle = \prod_i |\psi\rangle_i$, where

$$|\psi\rangle_i = \sum_{n_i^a, n_i^b} f^i_{n_i^a, n_i^b} |n_i^a, n_i^b\rangle_i, \quad (2)$$

and $f^i_{n_i^a, n_i^b}$ are the Gutzwiller coefficients on site i. The variational energy of the system in terms of $f^i_{n_i^a, n_i^b}$ is given by $E = \langle \psi | H | \psi \rangle = E_0 + E_1 + E_2$, where

$$E_0 = \sum_i \sum_{n_i^a, n_i^b} \Big[\big(-\mu(n_i^a + n_i^b) + \Delta n_i^b + \frac{U}{2}\big[n_i^a(n_i^a - 1) + 2\lambda n_i^a n_i^b\big]\big) \Big| f^i_{n_i^a, n_i^b} \Big|^2 + \Omega\big(\sqrt{n_i^a(n_i^b + 1)}\, f^{i*}_{n_i^a - 1, n_i^b + 1} f^i_{n_i^a, n_i^b} + \text{H.c.}\big) \Big]$$

$$E_1 = -J/2 \sum_{\langle ij \rangle} \sum_{n^a_{i,j}, n^b_{i,j}} \Big[\Big(f^{i*}_{n_i^a - 1, n_i^b} f^{j*}_{n_j^a + 1, n_j^b} \sqrt{n_i^a(n_j^a + 1)} + \eta f^{i*}_{n_i^a, n_i^b - 1} f^{j*}_{n_j^a, n_j^b + 1} \Big) f^i_{n_i^a, n_i^b} f^j_{n_j^a, n_j^b} + \text{H.c.} \Big]$$

$$E_2 = V_{\text{di}}/2 \sum_{\langle ij \rangle} \sum_{n^a_{i,j}, n^b_{i,j}} \Big| f^i_{n_i^a, n_i^b} f^j_{n_j^a, n_j^b} \Big|^2 n_i^b n_j^b. \quad (3)$$

A numerical minimization E provides the mean-field ground states. We note that for finite Ω, H conserves $n_i = n_i^a + n_i^b$; however, n_i^a and n_i^b are not conserved. It is evident from Eq. (1) that n_i in the ground state is determined by μ; in contrast, n_i^b for a fixed μ is determined by a competition between $\Delta < 0$ and V_{di} which are optimized by $n_i^b = 1$ on every site and $n_i^b = 0$ on every alternate site, respectively. This competition provides a possibility of translational-symmetry-broken ground states with two-sublattice structure (denoted subsequently as A and B). These expectations are corroborated in the phase diagrams shown in Figs. 1 and 2 for representative values of the parameter for $n_i \leqslant 2$ at each site. We find from Fig. 1 that for $n_i \leqslant 1$, the Mott phases constitute "uniform Mott-insulating" (UMI) phases with $n_i = 0$ and 1 at each lattice site, and two-sublattice symmetry-broken DW and CIAF phases. For the DW phase, the A sublattice has a linear combination of $|1,0\rangle$ and $|0,1\rangle$ states where the B sublattice has $n_i = 0$, leading to $n_A - n_B = 1$ and $\bar{n} = (n_A + n_B)/2 = 1/2$. The CIAF phase, in contrast, has $n_A = n_B = 1$; in this phase the Gutzwiller wave function takes the form

$$|\psi_{A(B)}\rangle = \cos(\theta_{A(B)})|1,0\rangle - \sin(\theta_{A(B)})|0,1\rangle, \quad (4)$$

on A (B) sublattice with the canting angle $\phi = \theta_A - \theta_B$. A schematic representation of these two phases is shown in Fig. 3. We note here that a Mott phase with general filling n_0, which is commonly known as "frozen Rydberg atoms,"

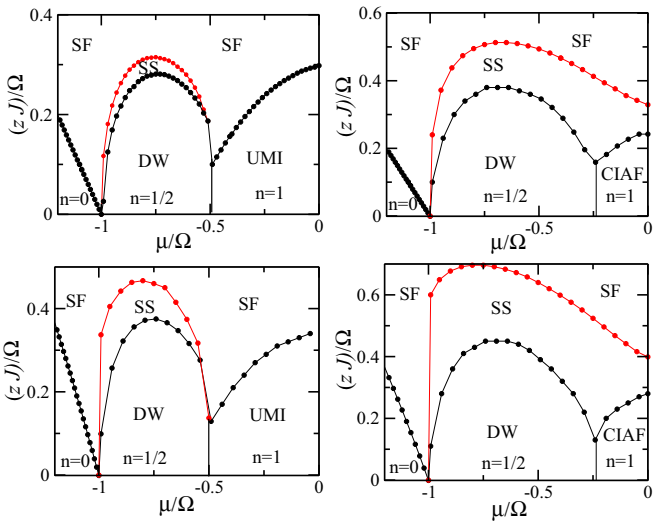

FIG. 1. (Color online) Top left (right): μ vs J phase diagram for $\mu < 0, \eta = 1, \Delta = 0, U/\Omega = 1, \lambda = 3$, and $zV_{\text{di}}/\Omega = 4$ (9) showing DW, SF, UMI, SS, and CIAF phases. Bottom: Same as the top panels but with $\eta = 0$.

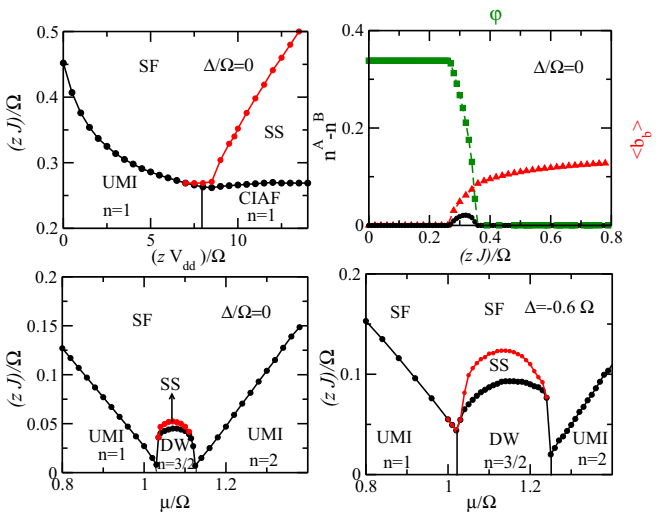

FIG. 2. (Color online) Top left: Phase diagram as a function of V_d and J for $\mu/\Omega = 0.2$ showing a multicritical point for $ZV_d/\Omega \simeq 8$ and $ZJ/\Omega \simeq 0.26$. Top right: Plot of the DW (black circle) and SS (red triangle) order parameter and cant angle ϕ (green square) as a function of J for $zV_d/\Omega = 10$ and $\mu/\Omega = 0.2$ across the CIAF-SS-SF transition. Bottom: μ vs J phase diagrams for $zV_d/\Omega = 4$ showing the DW with $\langle n\rangle = 3/2$, uniform MI, SS, and SF phases. For all plots, $\eta = 1$, $\lambda = 3$, and $U/\Omega = 1$.

can be described by an effective spin Hamiltonian [5],

$$H_{\rm spin} = \Omega \sum_i [|\uparrow\rangle\langle\downarrow|_i + |\downarrow\rangle\langle\uparrow|_i] + \sum_{\langle ij\rangle} P_i V_{ij} P_j + \Delta \sum_i |\uparrow\rangle\langle\uparrow|_i, \quad (5)$$

where the ground (excited) state is denoted by pseudospin down (up) states $|\downarrow\rangle = |n_0,0\rangle$, $|\uparrow\rangle = |n_0-1,1\rangle$, and $P = |\uparrow\rangle\langle\uparrow|$ is the projector for the excited state. The above model belongs to the antiferromagnetic Ising class and captures the transition from the uniform MI phase to the CIAF phase, which is a continuous transition. For van der Waals interactions V_{ij} falls off faster than $1/|i-j|^2$; hence, the interaction can be considered "short ranged" and the nearest-neighbor Ising spin interaction plays the crucial role. The CIAF phase is favored over the uniform MI phase for $zV_{\rm di} \geqslant zV_{\rm di}^c/\Omega \simeq 8$ as can be seen from the top left panel of Fig. 2.

From Fig. 1, we also find that, upon increasing J, one encounters two second-order transitions; the first occurs from the DW or CIAF phases to a SS phase with $n_A \neq n_B$ and $\langle b_a\rangle, \langle b_b\rangle \neq 0$ and the second from the SS phase to a uniform SF phase. The DW and the SF order parameters and the CIAF canting angle across the CIAF-SS-SF transition are shown in right-hand panel of Fig. 2 for $zV_{\rm di}/\Omega = 10$ and $\mu/\Omega = 0.2$. We also find the existence of several multicritical points in the phase diagram where SS, SF, and DW (Fig. 1, left) and CIAF, SS, DW, and SF phases (Fig. 1, top right, and Fig. 2, top left) meet. The inclusion of fluctuation may lead to phase separation near such multicritical points; an analysis of this effect is beyond the scope of the present mean-field theory. A similar phase diagram for $\mu > 0$, shown in the bottom panel of Fig. 2, reveals the existence of an $\langle n\rangle = 3/2$ DW phase which

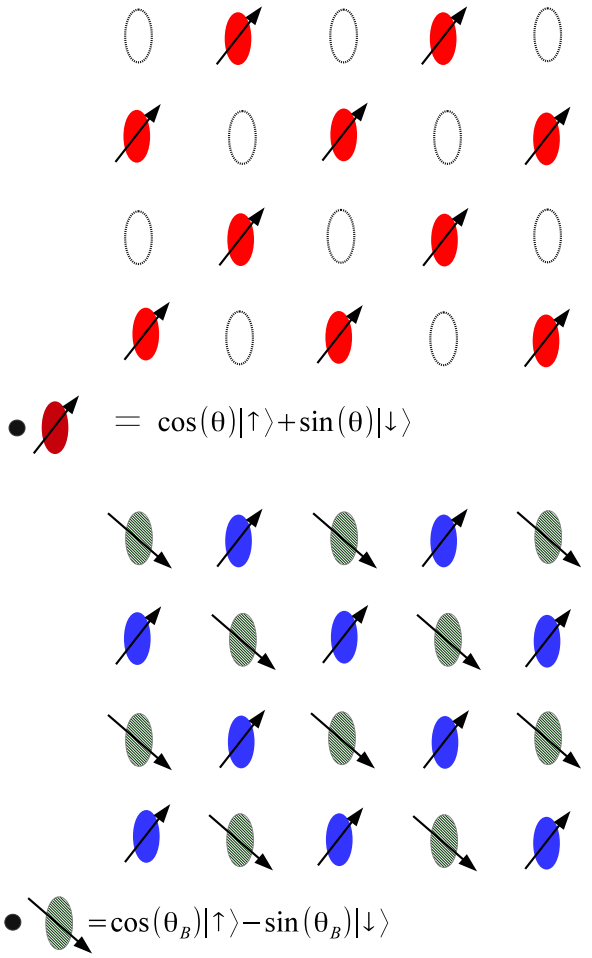

FIG. 3. (Color online) Schematic representation of the (top) DW and the (bottom) CIAF phases. The symbol $|\uparrow\rangle$ represents the state $|n_0-1,1\rangle$ in the MI phase with n_0 bosons on a given lattice site while $|\downarrow\rangle$ represents $|n_0,0\rangle$. The empty site indicates an absence of any boson on those sites.

has a linear combination of $|1,0\rangle$ and $|0,1\rangle$ ($|1,1\rangle$ and $|2,0\rangle$) states on the A (B) sublattice. We note from the bottom panels of Fig. 2 that the SS phase atop the $\langle n\rangle = 3/2$ DW phase is favored by large negative Δ.

III. PHASES AND EXCITATION SPECTRUM OF HARD-CORE RYDBERG ATOMS

In this section, we consider hard-core bosons ($U \gg \Omega, V_{\rm di}, \Delta$) with filling $n_i \leqslant 1$. In this regime, the single-site wave function can be written as

$$|\psi\rangle_i = f_{00}^i|0,0\rangle + f_{10}^i|1,0\rangle + f_{01}^i|0,1\rangle. \quad (6)$$

The simplicity of the single-site wave functions allows for analytical calculation of the phase diagram and excitation spectrum of the bosons, which is the main focus of the rest of the paper.

The ground-state phases can be obtained by minimizing the energy with respect to the variational parameters f^i, as described in the previous section. To study the dynamics and collective excitations of the bosons analytically, we

generalize Eq. (2) with time-dependent $f^i_{n_i^a,n_i^b}(t)$. The resulting Schrödinger equations for $f^i_{n_i^a,n_i^b}(t)$ can be obtained by minimizing the action

$$S = \int dt \langle \psi | i\partial_t - H | \psi \rangle \tag{7}$$

with the constraints $\sum_{n_i^a,n_i^b} |f^i_{n_i^a,n_i^b}|^2 = 1$ for each site. The dynamical equations of the variational parameters are given by

$$\begin{aligned}
i\dot{f}^i_{00} &= -Jf^i_{10}\sum_\delta f^\delta_{00} f^{*\delta}_{10} - J\eta f^i_{01}\sum_\delta f^\delta_{00} f^{*\delta}_{01} - \lambda_i f^i_{00},\\
i\dot{f}^i_{10} &= \Omega f^i_{01} - (\mu+\lambda_i) f^i_{10} - Jf^i_{00}\sum_\delta f^{*\delta}_{00} f^\delta_{10},\\
i\dot{f}^i_{01} &= \Omega f^i_{10} - (\mu-\Delta+\lambda_i) f^i_{01} + V_{\rm di} f^i_{01}\sum_\delta \left|f^\delta_{01}\right|^2\\
&\quad - J\eta f^i_{00}\sum_\delta f^{*\delta}_{00} f^\delta_{01},
\end{aligned} \tag{8}$$

where δ is the nearest-neighbor site index of the ith site and λ_i are the Lagrange multipliers corresponding to the wave-function normalization at each site. The ground-state phases of the system can also be obtained as the steady-state solutions $\bar{f}^i_{n_i^a,n_i^b}$ of the Schrödinger equation. Within the linear response regime the variational parameters at each site can be decomposed as $f^i_{n_i^a,n_i^b}(t) = \bar{f}^i_{n_i^a,n_i^b} + \delta f^i_{n_i^a,n_i^b}$, where $\bar{f}^i_{n_i^a,n_i^b}$ represents the steady-state solution of the dynamical equations corresponding to the ground state (mean-field solutions) and $\delta f^i_{n_i^a,n_i^b}$ are the time-dependent small amplitude fluctuations of the ground state. The eigenfrequencies ω of the small fluctuations $\delta \bar{f}^i e^{i\omega t}$ describe the collective excitations of the quantum phases and determine their stability [16].

Using this time-dependent variational technique, we obtained correlated phases of Rydberg excited atoms and their collective excitations in the hard-core limit. The detailed discussion on various phases and analytical results is presented separately in following sections. The details of these calculations can be found in the Appendix; here we present the key results regarding the different phases and their collective modes.

A. Uniform MI and SF phases

The uniform MI phase with $\langle n \rangle = 0$ is described by the wave function

$$|\mathrm{MI}, n=0\rangle = \prod_i f^i_{00} |0,0\rangle_i, \tag{9}$$

with $f^i_{00} = 1$. For $J = 0$, this MI phase appears for $\mu < -\sqrt{\Omega^2 + \Delta^2/4} + \Delta/2$; with increasing J one finds a continuous transition to a uniform SF phase. The particle excitations are described by the fluctuations δf^i_{10} and δf^i_{01} with energy

$$\omega_{\vec{k}} = \pm\sqrt{\frac{1}{4}\{\Delta + (1-\eta)\epsilon_{\vec{k}}\}^2 + \Omega^2} + \frac{\Delta}{2} - \mu - (1+\eta)\epsilon_{\vec{k}},$$

where $\epsilon_{\vec{k}} = 2J\sum_{i=1}^d \cos(k_i)$. The phase boundary between the MI and the SF phases which can be obtained from the condition $\omega_{\vec{k}=0} = 0$ is shown in the top left of Fig. 4.

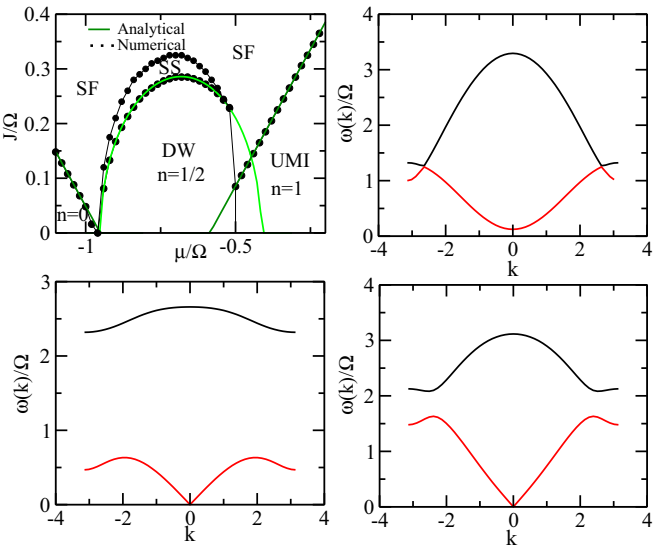

FIG. 4. (Color online) Top left: Analytical phase diagram for $\mu < 0$ in the hard-core limit. All parameters except U and λ are the same as the top left of Fig. 1. Top right: Excitation spectra of the uniform MI $V/\Omega = 1$, $J/\Omega = \Delta/\Omega = 0.1$, $\mu/\Omega = 0.2$, $z = 6$, and $\eta = 1$. Bottom: Excitation spectra of the SF phase over the SS phase (left) and uniform MI phase (right). All parameters are the same as those in the top right except $J/\Omega = 0.1$ (0.2) and $\mu/\Omega = -0.75$ (0.2) for the bottom left (right) panels. Here $k = |\vec{k}|$ along $k_x = k_y = k_z$.

For larger values of μ, a uniform MI phase with $n_i = 1$ occurs for $V_{\rm di} < V^c_{\rm di}$. In this phase the wave function at each site is given by

$$|\mathrm{MI}, n=1\rangle = \prod_i \left(f^i_{10}|1,0\rangle_i + f^i_{01}|0,1\rangle_i\right) \tag{10}$$

with $f^i_{10} = \cos\theta$ and $f^i_{01} = -\sin\theta$. The collective excitations of this MI phase are shown in the top right of Fig. 4. For $J > J_c$, the MI phase becomes unstable by the creation of holes with excitation energy,

$$\omega^h_{\vec{k}} = -\Omega f_{01}/f_{10} + \mu - J(|f_{10}|^2 + \eta|f_{01}|^2)\epsilon_{\vec{k}}, \tag{11}$$

and enters into a homogeneous SF phase via a second-order phase transition occurring at $\omega^h_{\vec{k}=0} = 0$ [17]. The collective modes of the SF phase are shown in the bottom right of Fig. 4 which displays the well-known massless phase and massive amplitude modes. Apart from the hole excitation, fluctuations in coherent superposition of ground and Rydberg excited states gives rise to pseudospin excitation mode. The pseudospin excitation energy of this phase is given by (see Appendix for details)

$$\omega^2 = \Omega^2\left[f^2_{01}/f^2_{10} + f^2_{10}/f^2_{01} - 2V_{\rm di} f_{10} f_{01}\epsilon_{\vec{k}}/(\Omega J) + 2\right]. \tag{12}$$

An instability occurs at a critical strength of van der Waals interaction $V_{\rm di}$ for which $\omega = 0$ at $\vec{k} = \pi$. This indicates broken translational symmetry in the uniform phase and appearance of antiferromagnetic ordering. The phase diagram so obtained agrees well with the numerical result for the MI-CIAF transition presented earlier.

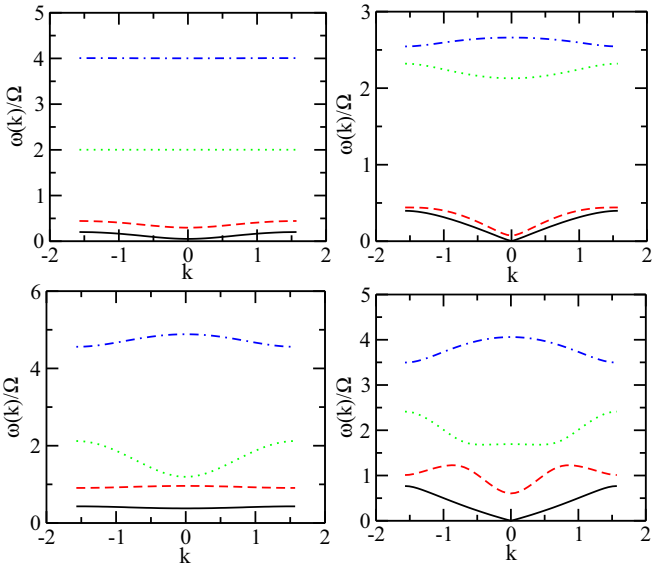

FIG. 5. (Color online) Top: Excitation spectra of the DW phase (left) and the nearest SS phase (right). The green dotted and blue dash-dotted lines denote the pseudospin excitation modes while the black solid and the red dashed lines denote particle-hole excitation modes. All parameters are same as those in the bottom left of Fig. 4 except $J/\Omega = 0.05$ (left) and 0.07 (right). Bottom: Excitation spectra of the CIAF phase (left) and that of its adjacent SS phase (right). All parameters are same as those in the top right of Fig. 4 except $V/\Omega = 2$ and $J/\Omega = 0.03$ (left) and 0.15 (right).

B. Density wave with half filling

The DW state with $\langle n \rangle = 1/2$ has only one boson per site on sublattices A whose wave function is given by

$$|\psi_A\rangle = \cos\theta|1,0\rangle - \sin\theta|0,1\rangle, \tag{13}$$

with $\tan 2\theta = 2\Omega/\Delta$ and an empty sublattice B (with $f_{00} = 1$). In the hard-core limit, the particles in sublattice A have an excited state $\sin\theta|1,0\rangle + \cos\theta|0,1\rangle$ with excitation energy $2\sqrt{\Omega^2 + \Delta^2/4}$. These can be thought of pseudospin flip excitation. For $J = 0$, another possible excitation is creation of a hole in sublattice A which costs an energy

$$E_h = \mu + \sqrt{\Omega^2 + \Delta^2/4} - \Delta/2. \tag{14}$$

Similarly at sublattice B particle excitation in two internal states (corresponding to pseudospin $\pm$) has energy

$$E_{p\pm} = -\mu + x/2 \pm \sqrt{x^2/4 + \Omega^2} \tag{15}$$

with $x = V_{\rm di} z \sin^2\theta + \Delta$. For finite J, the particle and hole excitations gain dispersions as shown in the top left of Fig. 5; however, the pseudospin modes remain dispersionless and well separated from the particle and hole modes. By increasing J, the DW state enters into a SS phase at $J = J_c$ via a continuous transition. The phase boundary between the DW and the SS phases can be obtained analytically by demanding the condition of one gapless excitation [17] and is given by

$$E_h E_{p+} E_{p-} = (zJ)^2[\eta\Omega \sin 2\theta + (x-\mu)\cos^2\theta - \mu(\eta \sin\theta)^2]. \tag{16}$$

For larger μ, the DW phase undergoes first-order transitions to SF ($J > J_c$) or MI ($J < J_c$) provided $V_{\rm di} < V_{\rm di}^c$. The collective modes of the SF phase are shown in the bottom left of Fig. 4 which displays the well-known gapless Goldstone mode. For $V_{\rm di} > V_{\rm di}^c$ and $J < J_c$, there is a continuous transition between the DW and the CIAF phases. The phase diagrams obtained from this analysis are shown in the top left of Fig. 4.

C. Canted Ising antiferromagnetic phase

In this phase each site has $\langle n \rangle = 1$ but with different linear combinations of the pseudospin up and down states in the two sublattices leading to a canting angle ϕ as explained earlier. Due to the two-sublattice structure, the hole excitation energies over this ground state are given by (see Appendix for a derivation)

$$\omega_\pm^h = -y_+/2 + \mu \pm \left[\left(f_{10}^A f_{10}^B + \eta f_{01}^A f_{01}^B\right)^2 \epsilon_k^2 + y_-^2/4\right]^{1/2},$$

where $y_\pm = \Omega[f_{01}^A/f_{10}^A \pm f_{01}^B/f_{10}^B]$. The CIAF phase melts when $\omega_-^h(k=0) = 0$, and a SS phase is formed; the corresponding phase diagram agrees well with the numerical result plotted in top left of Fig. 2. The CIAF phase also has two gapped pseudospin excitations (bottom left of Fig. 5); their analytical expression for general filling n_0 per site is given in the Appendix and reads

$$\omega^2 = \beta_1 \pm \sqrt{\beta_2^2 + (\gamma_+^2 - \gamma_-^2)\epsilon_k^2}, \tag{17}$$

where the parameters can be expressed in terms of the variational parameters of the wave functions in two sublattices,

$$\begin{aligned} \beta_1 &= 2\Omega^2 n_0[2 + \cot^2 2\theta_A + \cot^2 2\theta_B], \\ \beta_2 &= 2\Omega^2 n_0[\cot^2 2\theta_A - \cot^2 2\theta_B], \\ \gamma_\pm &= -\Omega\sqrt{n_0} V_{\rm di}(\sin 2\theta_A \pm \sin 2\theta_B)/(2J). \end{aligned} \tag{18}$$

In contrast to the DW phase, the CIAF pseudospin modes have finite dispersion and the lower pseudospin mode is close to the higher hole excitation branch. Consequently, the SS phase above CIAF shows a "roton"-like structure resulting from the hybridization of these modes.

D. Supersolid phase

One of the most interesting states of matter is the "supersolid phase," which is yet to be observed in experiments. Ultracold Rydberg atoms with long-range interaction are a possible candidate for supersolidity. In the DW and CIAF phases the lattice translational symmetry is broken due to the van der Waals interaction. These insulating phases form the backbone structure of supersolid phases. The DW melts due to the particle-hole excitations and undergoes a second-order transition to the SS phase. In this SS phase, the holelike excitations are well separated in energy from the pseudospin flip excitations; their dispersion is shown in the top right of Fig. 5. Due to the hole excitations the CIAF phase melts and a SS phase is formed through a continuous transition. Since the CIAF phase has uniform density, the SS phase above it has a relatively small density oscillation compared to that above the DW phase. The SS phase above the CIAF phase, in contrast to its counterpart obtained from the DW phase, displays a preformed rotonlike structure resulting from the

hybridization of these hole and pseudospin excitation branches as depicted in bottom right of Fig. 5. Thus these SS phases can be distinguished by their collective mode structure.

IV. CONCLUSION

The experimental verification of the collective modes and the phase diagram predicted in this work would involve standard experiments carried out on ultracold-atom systems [13,18,19]. Usual momentum distribution measurements would differentiate between the predicted MI and the SS or SF phases. The DW phase can be distinguished from the CIAF and the uniform MI phases by the presence of a checkerboard pattern showing odd and even occupation in alternate sites belonging to different sublattices; such a pattern can be easily measured in parity of occupation measurement of individual sites [13]. The distinction between the SS phases obtained by increasing J starting from CIAF and DW phases would requires measurement of the dispersion of the collective modes via lattice modulation or Bragg spectroscopy experiments [19,20]. The SS phases would display both a checkerboard pattern for occupation numbers and a momentum distribution peak at $k = 0$ which would distinguish it from other phases.

The details of the experimental parameters typically used for experiments with Rydberg atoms in a lattice are as follows. For a 1D lattice of such atoms with 100 sites, it has been possible to excite 50 atoms in the Rydberg states, which leads to a blockade radius of one or two lattice spacings with typical lattice spacing of 0.4 μm [12]. We envisage a similar blockade radius for the higher-dimensional lattices. The typical Rabi frequency used is $\sim$200–500 kHz and the detuning Δ can be varied to be small or large with respect to Ω. The dipole interaction can be tuned between 0.5 and 10 MHz or higher, leading to a ratio of $V_{\rm di}/\Omega \sim$ 1–50. The hopping parameter J can be easily varied between 1 and 100 kHz by varying the lattice depth. We note that these parameters indicate that the DW, CIAF, and SS phases can be easily obtained in experiments. In this context, we would like to note that the typical hopping time for the atoms ($\sim\hbar/J$) is much larger than the lifetime of the Rydberg atoms; thus the experiments are typically carried out in the regime where the excited atoms are frozen. This corresponds to the $\eta = 0$ limit of our analysis.

We note that this work presents a preliminary study of the possible phases and collective excitations of correlated Rydberg atoms in an optical lattice, based on a simplified model. Due to the true long-range nature of van der Waals interactions, various density-wave phases can form in between the $n = 0$ MI phase and the DW phase with $n = 1/2$. These insulating phases have a filling factor $1/n$ (where n is an integer) and form a "devil's staircase"-like structure [21]. Apart from the checkerboard pattern, a "stripe supersolid" may form for next-nearest-neighbor interactions. Also the "roton" minimum may shift to smaller momentum (instead of $\pm\pi$) due to true long-range interaction. In the real experimental setup the lifetime and stability of these equilibrium phases are very much dependent on the decay rate of the highly excited Rydberg atoms. Such decay times increase with the principal quantum number n' of the atoms in the lattice and can thus be made large. A typical experimental estimate of such a lifetime can be as large as 50 μs for Rb atoms. A more accurate analysis requires a time-dependent calculation including the decay time of the Rydberg atoms which we do not attempt here.

To conclude, we have charted out the mean-field phase diagram and computed the collective modes of laser-driven Rydberg atoms. Our work, which is expected to be qualitatively accurate for $d \geqslant 2$, has demonstrated the presence of SS, CIAF, and DW phases of these atoms which have distinct collective mode spectra. We note that the CIAF phase found here constitutes an example of a translation-symmetry-broken magnetic ground state in a $d > 1$ ultracold-atom system. Possible extension of our work would involve study of the effect of quantum fluctuations on the mean-field phase diagram and a more detailed incorporation of the effect of the dipolar interaction between the Rydberg atoms which is expected to be important for $V_{\rm di} \gg \Omega, \Delta, J, U$. We have suggested several experiments to test our theory.

APPENDIX

Here we provide the details of the analytical calculations used to determine the phase boundaries and the collective modes of the Rydberg atoms in an optical lattice in the hard-core limit. To analyze the phases and the collective modes of a system of Rydberg atoms described by H defined in Eq. (1), we consider the hard-core bosons with $U \to \infty$. In this limit the Gutzwiller wave function at any site i can be written as $|\psi\rangle_i = f^i_{00}|0,0\rangle + f^i_{1,0}|1,0\rangle + f^i_{01}|0,1\rangle$. The mean-field energy of the system is given by

$$\begin{aligned} E[\{f^i\}] = \Omega \sum_i \left[f^{i*}_{10} f^i_{01} + f^{i*}_{01} f^i_{10}\right] - \mu \sum_i \left[\left|f^i_{10}\right|^2 + \left|f^i_{01}\right|^2\right] \\ + \Delta \sum_i \left|f^i_{01}\right|^2 + \frac{V_{\rm di}}{2} \sum_{\langle ij\rangle} \left|f^i_{01}\right|^2 \left|f^j_{01}\right|^2 \\ - J \sum_{\langle ij\rangle} f^{i*}_{00} f^i_{10} f^j_{00} f^{j*}_{10} - J\eta \sum_{\langle ij\rangle} f^{i*}_{00} f^i_{01} f^j_{00} f^{j*}_{01}. \end{aligned} \tag{A1}$$

Using the time-dependent Gutzwiller wave function the action, given by Eq. (7), becomes

$$S = \int dt \left[i \sum_i \left\{ f^{i*}_{00} \dot{f}^i_{00} + f^{i*}_{10} \dot{f}^i_{10} + f^{i*}_{01} \dot{f}^i_{01} \right\} - E[\{f^i\}] \right]. \tag{A2}$$

The Schrödinger equation for $f^i(t)$ can be easily derived by variation of Eq. (A2) with respect to $f^{i*}(t)$ and yields Eq. (8). To find the frequencies of the small fluctuations using Eq. (8), we decompose each f^i in two parts, $f^i(t) = \bar{f}^i + \delta f^i(t)$. The steady-state solutions of Eq. (8) corresponding to the ground state of the system are $\bar{f}^i$, and $\delta f^i(t)$'s are time-dependent small amplitude fluctuations around the steady-state values. We decompose these fluctuations in Fourier modes $\delta f^j = e^{-i\omega t} \sum_k e^{i\vec{k}\cdot\vec{R}_j} \delta f(\vec{k})$ to obtain the collective frequencies $\omega(\vec{k})$ from the linearized dynamical equations [Eq. (8)]. For the phases with two-sublattice structure, we have used the notation $\bar{f}^j = f^s + f^a e^{i\vec{\pi}\cdot\vec{R}_j}$ and $\lambda_j = \lambda_s + \lambda_a e^{i\vec{\pi}\cdot\vec{R}_j}$, where $\vec{R}_j$ is the position of lattice site j.

1. State with $n = 0$

In this state, $\bar{f}_{00} = 1$, $\bar{f}_{10} = 0$, $\bar{f}_{01} = 0$. From the steady-state solution of the equation of motion we obtain $\lambda_i = 0$ for all sites. The particle excitations can be obtained from the linearized equations for δf:

$$\omega\delta f_{10}(\vec{k}) = \Omega\delta f_{01}(\vec{k}) - \mu\delta f_{10}(\vec{k}) - \epsilon_{\vec{k}}\delta f_{10}(\vec{k}), \quad \text{(A3)}$$

$$\omega\delta f_{01}(\vec{k}) = \Omega\delta f_{10}(\vec{k}) - (\mu - \Delta)\delta f_{01}(\vec{k}) - \eta\epsilon_{\vec{k}}\delta f_{01}(\vec{k}), \quad \text{(A4)}$$

which leads to the particle excitations with two internal degrees, given by

$$\omega_k = \pm\sqrt{\{\Delta + (1-\eta)\epsilon_{\vec{k}}]^2/4 + \Omega^2} + \frac{\Delta}{2} - \mu - (1+\eta)\epsilon_{\vec{k}}/2, \quad \text{(A5)}$$

where $\epsilon_{\vec{k}} = 2J\sum_{i=1}^{d}\cos(k_i)$. The instability of this phase takes place for $k = 0$, leading to the formation of a homogeneous SF phase. The phase boundary is given by

$$(\mu + Jz)(\mu - \Delta + J\eta z) = \Omega^2. \quad \text{(A6)}$$

2. DW state with $n = 1/2$

This DW state has a two-sublattice structure and the wave function is given by $|1,0,1,0,\ldots\rangle$. The sites of sublattice B are empty and $f_{00}^{B} = 1$. The particles at sublattice A are in linear superposition of the ground state and the Rydberg state, with $f_{10}^{A} = \cos\theta$ and $f_{01}^{A} = -\sin\theta$. The minimization of $E[\{f^i\}]$ gives $\tan 2\theta = 2\Omega/\Delta$. From the steady-state condition obtained from equating the right-hand side of Eq. (8) to zero, we can fix the Lagrange multipliers to be $\lambda^A = -\mu + \Delta/2 - \sqrt{\Delta^2/4 + \Omega^2}$ and $\lambda^B = 0$. In momentum space the linearized equations for fluctuations can thus be written as

$$\begin{aligned}
-\omega\delta f_{00}^{*+}(\vec{k}) &= -2f_{10}^{S}\epsilon_{\vec{k}}\delta f_{10}^{-}(\vec{k}) - 2\eta f_{01}^{S}\epsilon_{\vec{k}}\delta f_{01}^{-}(\vec{k}) \\
&\quad - 2\lambda_S\delta f_{00}^{*+}(\vec{k}), \\
\omega\delta f_{10}^{-}(\vec{k}) &= \Omega\delta f_{01}^{-}(\vec{k}) - \mu\delta f_{10}^{-}(\vec{k}) - 2f_{10}^{S}\epsilon_{\vec{k}}\delta f_{00}^{*+}(\vec{k}), \\
\omega\delta f_{01}^{-}(\vec{k}) &= \Omega\delta f_{10}^{-}(\vec{k}) - (\mu - \Delta)\delta f_{01}^{-}(\vec{k}) \\
&\quad + 4V_{\mathrm{di}}z\left|f_{01}^{S}\right|^2\delta f_{01}^{-}(\vec{k}) - 2\eta f_{01}^{S}\epsilon_{\vec{k}}\delta f_{00}^{*+}(\vec{k}),
\end{aligned} \quad \text{(A7)}$$

where $\delta f^{\pm}(\vec{k}) = \delta f(\vec{k}) \pm \delta f(\vec{k} + \vec{\pi})$ and $\lambda_S = (\lambda^A + \lambda^B)/2$. We note that δf^{i*} satisfies similar equations with ω replaced by $-\omega$. In the atomic limit, for $J = 0$ we obtain the particle (hole) excitations of sublattice B (A) analytically from the above equations. Removing a particle from sublattice A (hole excitation) costs an energy $E_h = \mu + \sqrt{\Omega^2 + \Delta^2/4} - \Delta/2$. This is the eigenvalue of fluctuations δf_{00}^{+}. The particle excitations in sublattice B can be obtained by diagonalizing the single-site atomic Hamiltonian written in the basis of $|1,0\rangle$ and $|0,1\rangle$ states. Particle excitation in two internal states has energy $E_{p\pm} = -\mu + x/2 \pm \sqrt{x^2/4 + \Omega^2}$ with $x = 4V_{\mathrm{di}}zf_{01}^{S2} + \Delta$. These are the eigenvalues corresponding to the fluctuations f_{01}^{-} and f_{10}^{-} in Eq. (A7). For nonvanishing J the eigenvalues can be obtained by numerically solving the cubic equation. For a second-order transition to the SS phase, the phase boundary can be obtained from the condition of vanishing eigenvalue at $k = 0$ and the analytical expression can be obtained from the determinant of the eigenvalue equations which can be read off from Eq. (A7),

$$\begin{aligned}
&2\lambda_S[\mu(\mu - x) - \Omega^2] \\
&\quad = 4J^2z^2\left[2\eta\Omega f_{10}^{S}f_{01}^{S} + \eta^2 f_{01}^{S2}\mu + f_{10}^{S2}(\mu - x)\right],
\end{aligned} \quad \text{(A8)}$$

where $x = 4V_{\mathrm{di}}zf_{01}^{S2} + \Delta$. From the expressions of $E_{p\pm}$ and E_h written earlier and using $f_{10} = \cos(\theta)$ and $f_{01} = -\sin(\theta)$, it can be shown that this condition is equivalent to $E_hE_{p+}E_{p-} = (zJ)^2[\eta\Omega\sin 2\theta + (x-\mu)\cos^2\theta - \mu(\eta\sin\theta)^2]$, which is used in the main text.

3. Uniform MI phase with $n = 1$

In this phase each site contains exactly one particle, which is a linear superposition of the ground state and the excited state. In this phase, one has at each site $f_{00} = 0$, $f_{10} = \cos\theta$, and $f_{01} = \sin\theta$, and θ can be obtained by minimizing the energy,

$$E/N = \Omega\sin 2\theta + \frac{V_{\mathrm{di}}z}{2}\sin^4\theta + \Delta\sin^2\theta. \quad \text{(A9)}$$

The Lagrange multiplier is given by $\lambda = \Omega f_{01}/f_{10} - \mu$. The excitation energy corresponding to the fluctuation δf_{00} is given by

$$\omega\delta f_{00}(\vec{k}) = -[(|f_{10}|^2 + \eta|f_{01}|^2)\epsilon_{\vec{k}} + \lambda]\delta f_{00}(\vec{k}). \quad \text{(A10)}$$

The transition from uniform Mott insulator to SF takes place due to the instability at $k = 0$ at $Jz(|f_{10}|^2 + \eta|f_{01}|^2) = \mu - \Omega f_{01}/f_{10}$. The spin excitations can be obtained from the linearized equations,

$$\omega\delta f_{10}(\vec{k}) = \Omega\delta f_{01}(\vec{k}) - (\mu + \lambda)\delta f_{10}(\vec{k}), \quad \text{(A11)}$$

$$\begin{aligned}
\omega\delta f_{01}(\vec{k}) &= \Omega\delta f_{10}(\vec{k}) - (\mu - \Delta + \lambda)\delta f_{01}(\vec{k}) \\
&\quad + V_{\mathrm{di}}z|f_{01}|^2\delta f_{01}(\vec{k}) + V_{\mathrm{di}}f_{01}^2(\epsilon_{\vec{k}}/J) \\
&\quad \times [\delta f_{01}(\vec{k}) + \delta f_{01}^{*}(\vec{k})].
\end{aligned} \quad \text{(A12)}$$

The energy of these excitations can be easily calculated to yield

$$\omega^2 = \Omega^2\left[\frac{f_{01}^2}{f_{10}^2} + \frac{f_{10}^2}{f_{01}^2} - \frac{2V_{\mathrm{di}}f_{10}f_{01}\epsilon_{\vec{k}}}{\Omega J} + 2\right]. \quad \text{(A13)}$$

4. Canted Ising antiferromagnetic phase with $n = 1$

In this phase each site has one particle but this phase has antiferromagnetic order. In this phase we have two sublattice

values of f_{10} and f_{01}. Fluctuation of f_{00} is given by

$$\omega\delta f_{00}(\vec{k}) = -\beta\epsilon_{\vec{k}}\delta f_{00}(\vec{k}) - \lambda_s\delta f_{00}(\vec{k}) - \lambda_a\delta f_{00}(\vec{k}+\vec{\pi}), \tag{A14}$$

$$\omega\delta f_{00}(\vec{k}+\vec{\pi}) = \beta\epsilon_{\vec{k}}\delta f_{00}(\vec{k}+\vec{\pi}) - \lambda_s\delta f_{00}(\vec{k}+\vec{\pi}) - \lambda_a\delta f_{00}(\vec{k}), \tag{A15}$$

with $\beta = (|f^s_{10}|^2 - |f^a_{10}|^2) + \eta(|f^s_{01}|^2 - |f^a_{01}|^2)$. The Lagrange multipliers are $\lambda_s = \Omega(f^A_{01}/f^A_{10} + f^B_{01}/f^B_{10})/2 - \mu$ and $\lambda_a = \Omega(f^A_{01}/f^A_{10} - f^B_{01}/f^B_{10})/2$. The hole excitation energy is given by

$$\omega^h_{\pm} = -\lambda_s \pm \sqrt{\beta^2\epsilon^2_{\vec{k}} + \lambda^2_a}. \tag{A16}$$

A straightforward substitution for β, λ_s, and λ_a in Eq. (A16) leads to Eq. (6) used in the main text.

The phase boundary can be obtained from the instability of the above excitation at $k = 0$, $\beta^2 z^2 = \lambda^2_s - \lambda^2_a$. The spin modes can be obtained from the fluctuations δf_{10} and δf_{01},

$$\omega\delta f_{10}(\vec{k}) = \Omega\delta f_{01}(\vec{k}) - (\mu + \lambda_s)\delta f_{10}(\vec{k}) - \lambda_a\delta f_{10}(\vec{k}+\vec{\pi}), \tag{A17}$$

$$\begin{aligned}\omega\delta f_{01}(\vec{k}) = {} & \Omega\delta f_{10}(\vec{k}) - (\mu - \Delta + \lambda_s)\delta f_{01}(\vec{k}) \\ & - \lambda_s\delta f_{01}(\vec{k}+\vec{\pi}) + V_{\rm di}z(|f^s_{01}|^2 + |f^a_{01}|^2) \\ & \times \delta f_{01}(\vec{k}) - V_{\rm di}z(2f^s_{01}f^a_{01})\delta f_{01}(\vec{k}+\vec{\pi}) \\ & + V_{\rm di}(|f^s_{01}|^2 - |f^a_{01}|^2)[\epsilon_{\vec{k}}/J] \\ & \times [\delta f_{01}(\vec{k}) + \delta f^{\star}_{01}(\vec{k})].\end{aligned} \tag{A18}$$

A similar set of equations can be obtained for $\delta f(\vec{k}+\vec{\pi})$ (replacing $\vec{k} \to \vec{k}+\vec{\pi}$ in the above equations) and for δf^* (taking the complex conjugate of the above equations and replacing ω by $-\omega$).

The spin modes can also be obtained for a CIAF phase with general filling $\langle n\rangle = n_0$ from a simple variational calculation. The variational wave function at the ith site can be written as

$$|\psi\rangle_i = \cos\theta_i|n_0,0\rangle + e^{i\phi_i}\sin\theta_i|n_0-1,1\rangle. \tag{A19}$$

The Lagrangian is given by

$$\begin{aligned}L = {} & \sum_i \big[\dot{\phi}_i\sin^2\theta_i + \Omega\sqrt{n_0}\sin 2\theta_i\cos\phi_i \\ & + U(n_0-1)(\cos^2\theta_i + \lambda\sin^2\theta_i)\big] \\ & + \frac{V_{\rm di}}{2}\sum_{i\neq j}\sin^2\theta_i\sin^2\theta_j + \frac{U}{2}(n_0-1)(n_0-2).\end{aligned} \tag{A20}$$

From variation of the Lagrangian we obtain following equations:

$$\dot{\theta}_i = -\Omega\sqrt{n_0}\sin\phi_i, \tag{A21}$$

$$\sin 2\theta_i\dot{\phi}_i + 2\Omega\sqrt{n_0}\cos 2\theta_i\cos\phi_i + V_{\rm di}\sin 2\theta_i\sum_{\delta}\sin^2\theta_i + U(\lambda-1)(n_0-1)\sin 2\theta_i = 0. \tag{A22}$$

After linearization and eliminating $\delta\phi$, we obtain

$$\omega^2\delta\theta_{\vec{k}} = \beta_1\delta\theta_{\vec{k}} + \gamma_+\epsilon_{\vec{k}}\delta\theta_{\vec{k}} + \beta_2\delta\theta_{\vec{k}+\vec{\pi}} + \gamma_-\epsilon_{\vec{k}}\delta\theta_{\vec{k}+\vec{\pi}}, \tag{A23}$$

$$\omega^2\delta\theta_{\vec{k}+\vec{\pi}} = \beta_1\delta\theta_{\vec{k}+\vec{\pi}} - \gamma_+\epsilon_{\vec{k}}\delta\theta_{\vec{k}+\vec{\pi}} + \beta_2\delta\theta_{\vec{k}} - \gamma_-\epsilon_{\vec{k}}\delta\theta_{\vec{k}}, \tag{A24}$$

where

$$\begin{aligned}\beta_1 &= 2\Omega^2 n_0[2 + \cot^2 2\theta_A + \cot^2 2\theta_B], \\ \beta_2 &= 2\Omega^2 n_0[\cot^2 2\theta_A - \cot^2 2\theta_B], \\ \gamma_{\pm} &= -\Omega\sqrt{n_0}V_{\rm di}(\sin 2\theta_A \pm \sin 2\theta_B)/(2J).\end{aligned} \tag{A25}$$

The excitation energy of spin modes are thus given by

$$\omega^2 = \beta_1 \pm \sqrt{\beta^2_2 + (\gamma^2_+ - \gamma^2_-)\epsilon^2_{\vec{k}}}. \tag{A26}$$

This completes our derivation of the excitation spectra of the different phases of the hard-core bosons. We would like to note that we expect the qualitative nature of the spectra to remain unchanged for large $U/\Omega \gg 1$ where the particle modes with $n_i > 1$, neglected in the hard-core limit, are gapped out and do not play an essential role in determining the low-energy properties of the system.

[1] M. D. Lukin, M. Fleischhauer, R. Cote, L. M. Duan, D. Jaksch, J. I. Cirac, and P. Zoller, Phys. Rev. Lett. **87**, 037901 (2001); D. Jaksch, J. I. Cirac, P. Zoller, S. L. Rolston, R. Cote, and M. D. Lukin, *ibid.* **85**, 2208 (2000).

[2] E. Urban, T. A. Johnson, T. Henage, L. Isenhower, D. D. Yavuz, T. G. Walker, and M. Saffman, Nat. Phys. **5**, 110 (2009); A. Gaitan, Y. Miroshnychenko, T. Wilk, A. Chotia, M. Viteau, D. Comparat, P. Pillet, A. Browaeys, and P. Grangier, *ibid.* **5**, 115 (2009).

[3] F. Cinti, P. Jain, M. Boninsegni, A. Micheli, P. Zoller, and G. Pupillo, Phys. Rev. Lett. **105**, 135301 (2010).

[4] N. Henkel, R. Nath, and T. Pohl, Phys. Rev. Lett. **104**, 195302 (2010); J. Honer, H. Weimer, T. Pfau, and H. P. Büchler, *ibid.* **105**, 160404 (2010).

[5] R. Low, H. Weimer, U. Krohn, R. Heidemann, V. Bendkowsky, B. Butscher, H. P. Büchler, and T. Pfau, Phys. Rev. A **80**, 033422 (2009); H. Weimer, R. Low, T. Pfau, and H. P. Büchler, Phys. Rev. Lett. **101**, 250601 (2008).

[6] H. Weimer, M. Moller, I. Lesanovsky, P. Zoller, and H. P. Büchler, Nat. Phys. **6**, 382 (2010); H. Weimer, M. Muller, H. P. Büchler, and I. Lesanovsky, Quantum Inf. Process **10**, 885 (2011).

[7] T. Pohl, E. Demler, and M. D. Lukin, Phys. Rev. Lett. **104**, 043002 (2010); H. Weimer and H. P. Büchler, *ibid.* **105**, 230403 (2010).

[8] I. Lesanovsky and H. Katsura, Phys. Rev. A **86**, 041601(R) (2012); I. Lesanovsky, Phys. Rev. Lett. **106**, 025301 (2011).

[9] B. Olmos, R. González-Férez, and I. Lesanovsky, Phys. Rev. Lett. **103**, 185302 (2009).

[10] B. Vaucher, S. J. Thwaite, and D. Jaksch, Phys. Rev. A **78**, 043415 (2008).

[11] S. Ji, C. Ates, and I. Lesanovsky, Phys. Rev. Lett. **107**, 060406 (2011).

[12] M. Viteau, M. G. Bason, J. Radogostowicz, N. Malossi, D. Ciampini, O. Morsch, and E. Arimondo, Phys. Rev. Lett. **107**, 060402 (2011).

[13] Such states have been theoretically proposed and experimentally realized in 1D tilted lattice boson models. See S. Sachdev, K. Sengupta, and S. M. Girvin, Phys. Rev. B **66**, 075128 (2002); M. Kolodrubetz, D. Pekker, B. K. Clark, and K. Sengupta, *ibid.* **85**, 100505(R) (2012); W. S. Bakr, A. Peng, M. E. Tai, R. Ma, J. Simon, J. I. Gillen, S. Folling, L. Pollet, and M. Greiner, Science **329**, 547 (2010).

[14] R. Low, H. Weimer, J. Nipper, J. B. Balewski, B. Butscher, H. P. Büchler, and T. Pfau, J. Phys. B **45**, 113001 (2012).

[15] We expect the phases obtained to remain the same qualitatively even when this condition is mildly violated; see Ref. [9] for details.

[16] D. L. Kovrizhin, G. Venketeswara Pai, and S. Sinha, Europhys. Lett. **72**, 162 (2005).

[17] The analytical phase boundary obtained from this condition is valid only for continuous transition. This results in a mismatch of the phase boundaries between numerics and analytics at the phase boundary of the DW and uniform MI phases around $\mu/\Omega = -0.5$ as seen in top left of Fig. 4.

[18] M. Greiner, O. Mandel, T. Esslinger, T. W. Hansch, and I. Bloch, Nature (London) **415**, 39 (2002); C. Orzel, A. K. Tuchman, M. L. Fenselau, M. Yasuda, and M. A. Kasevich, Science **291**, 2386 (2001).

[19] D. Greif, L. Tarruell, T. Uehlinger, R. Jördens, and T. Esslinger, Phys. Rev. Lett. **106**, 145302 (2011); R. Sensarma, K. Sengupta, and S. Das Sarma, Phys. Rev. B **84**, 081101(R) (2011).

[20] P. T. Ernst, S. Gotze, J. S. Krauser, K. Pyka, D.-S. Lehmann, D. Pfannkuche, and K. Sengstock, Nat. Phys. **6**, 56 (2010); J. Stenger, S. Inouye, A. P. Chikkatur, D. M. Stamper-Kurn, D. E. Pritchard, and W. Ketterle, Phys. Rev. Lett. **82**, 4569 (1999); D. M. Stamper-Kurn, A. P. Chikkatur, A. Görlitz, S. Inouye, S. Gupta, D. E. Pritchard, and W. Ketterle, *ibid.* **83**, 2876 (1999).

[21] E. Sela, M. Punk, and M. Garst, Phys. Rev. B **84**, 085434 (2011).